Effects of H eterogeneous Mobility on D2D- and Drone-Assisted Mission-Critical MTC in 5G

Published version Digital Object Identifier 10.1109/TIM.2018.2866358

AN INDOOR ULTRASONIC SYSTEM FOR AUTONOMOUS 3D POSITIONING

Riccardo Carotenuto, *Member, IEEE,* Massimo Merenda, Demetrio Iero, Francesco G. Della Corte, *Senior Member, IEEE*

Dipartimento di Ingegneria dell'Informazione, delle Infrastrutture e dell'Energia Sostenibile,

Università degli Studi "Mediterranea" di Reggio Calabria,

Loc. Feo di Vito - 89060 REGGIO CALABRIA – ITALY

Abstract

Indoor positioning is an emerging technology with wide applications. Augmented and mixed reality need accurate and real time positioning of user's limbs or direction of sight in real time, and reference points within the real environment. Positioning is also required for mall navigation, elderly people movements monitoring, and many others contexts. Indoor positioning of mobile units (MU) can be provided by multilateration techniques that compute the location of a MU starting from distance measurements between the MU and a set of beacons. In this work, a nonlinear closed-form solution for the trilateration problem is employed to avoid heavy numerical iterative algorithms. The closed-form solution is allowed by a particular arrangement of the beacons, placed at the vertex of a square. A positioning system is presented where MUs, exploiting the light algorithm of the closed-form positioning, are able to autonomously and privately calculate their own positions. A prototype of the positioning system has been designed, realized and characterized for an average 4×4×3 m^3 home or office room. It includes four beacons that emit a sequence of ultrasonic chirp signals, several MUs, and a master unit that provides time synchronization via ANT transceivers on board each MU and the master unit. Thanks to the adopted closed form solution, each tiny battery-operated MU is able to carry out all the computations on-board, including analog and digital signal processing, beacon-MU distance estimation, and finally MU positioning at a rate of 2 Hz.

Index terms: Ultrasonic positioning, 3D positioning, chirp modulation, wireless communication, nonlinear equations

I. INTRODUCTION

Emerging technologies such as gestural interfaces, domotics, augmented and mixed reality, require accurate and fast positioning systems [1]. In the past years, ultrasonic positioning systems (UPS) have been demonstrated suitable for a variety of such applications, as they can provide positioning with sufficiently high rate and accuracy at a reasonably low cost.

Furthermore, an accurate positioning system able to localize an object with enough space and time resolution to allow accurate tracking in a given reference frame, is a technology that has recently enabled, or has potential to enable, a number of new applications in different fields of human life.

Fast and accurate UPS can be employed for virtual and augmented reality gestural interfaces [2]–[4], for human posture recognition and medical rehabilitation [5], [6], for indoor navigation [7], [8], for elderly and disabled people monitoring and assistance [9], etc. Applications include domotics, robotics, security, safety, preventing accidents through recognition of dangerous workers' postures and positions, logistics, tracking goods in warehouse, monitoring body and limb location during exercises for sport and military training, gaming consoles.

Typically, an ultrasonic positioning system is composed of a fixed reference infrastructure and a multiplicity of mobile units. Positioning is computed as a result of a two-step process. In the first step, the distances from each mobile unit and some fixed reference points (RPs) are measured. Afterwards, these distances are used to geometrically determine the position of each mobile in the reference system defined by the fixed RPs.

Distances can be measured with high accuracy and at a reasonable cost using ultrasonic signals. By knowing the sound speed in air, the distance can be obtained from the estimation of the travel time from an emitter to a receiver, i.e. the Time of Flight (*ToF*). *ToF* is the time elapsed from the instant a signal is transmitted to the instant of its arrival at the receiver. Precise distances measurements require a tight synchronization between the local clocks of the transmitter and the receiver. For example, a synchronization discrepancy of 100 μs corresponds to a distance uncertainty of 34.3 mm, with the sound speed of 343 m/s.

Different synchronization techniques have been proposed in literature [10], [11]. Multilateration uses the distances between RPs and the point to be localized as radii of spheres, at the intersection of which is the sought position. In 3D space, the minimum number of spheres, and therefore of RPs, is four, which decreases to three if the constraints of the problem allow us to consider positioning in a semi-space only. On the other hand, it is possible to use the information of additional distance measurements to refine the estimated position of the target, thereby making it less susceptible to measurement errors [12].

A free arrangement for the RPs yields an equation system, where each equation represents a sphere centered in one of the RP, whose radius is given by the distance between that RP and the MU. The MU position is found at the intersection of the spheres, i.e. as the solution of the nonlinear equation system. In general, this equation system has not a closed form solution, thus requiring the use of some numerical methods for solving. This results in a complex and iterative calculation, which is power and time consuming, without the guarantee that the solution found is the optimal one [13].

A number of positioning systems don't require emitter-receiver synchronization; the single distance between each RP and the mobile unit is not directly estimated, but instead the time difference between the arrivals of the signals emitted at the same time from many emitters, or time difference of arrival (*TDoA*), is measured [14]–[17]. The position is computed as the intersection of three hyperboloids. However, the hyperbolic formulation of the problem requires at least four RPs for 3D positioning within a half-space, while sphere intersection can do the same job with only three RPs. Moreover, hyperbolic solution of the *TDoA* localization problem is highly non linear in nature and much more sensitive to ranging errors than the spheres' intersection.

Due to its accurate and robust *ToF* estimation, cross-correlation is the most widely adopted technique. Cross-correlation measures the similarity of transmitted and received signals as a function of the time displacement of one relative to the other; the relative displacement yielding the maximum value corresponds to the *ToF*. By its integral nature, cross-correlation exploits all the information contained in the signals for estimation of the *ToF* [18].

Although single-tone signal is the easiest to generate and most suitable for feeding commercially available narrow-band ultrasonic transducers, environmental noise makes it difficult to detect the cross-correlation peak corresponding to the ToF since single-tone cross-correlation shows many adjacent peaks of similar amplitude. Among different techniques one of the most significant performance improvement is achieved by employing the linear chirp, which is a sinusoidal signal linearly sweeping frequency from f_{MIN} to f_{MAX} across the time interval T_{CHIRP} [19], [20]. In fact, the chirp cross-correlation shows a very sharp and easy to recognize peak.

This work aims to present an indoor positioning system showing centimeter level 3D positioning accuracy, sufficient for many of the room level positioning-based applications previously described. It uses RF time synchronization between emitter and receiver, ultrasonic chirp signal for *ToF* and distance estimation, and sphere intersection for point coordinates calculation.

The proposed system shows some new features: i) although the *ToA* is adopted, which can be done with just three RPs, four RPs are used here. They are arranged at the vertex of a flat square. With this arrangement, it was possible to use a closed form solution of the three spheres intersection [21]. ii) The adopted closed form solution and the characteristics of the mobile unit make it possible the on-board computation of the mobile own position in a totally autonomous and private way, in the sense that the positioning infrastructure is not aware of the presence and position of the MUs. iii) The distance measurements required for positioning are carried out through emitter-receiver synchronization using the standard ANT protocol, which was demonstrated for ranging in [22]. ANT units show very low power consumption, allowing MUs with small batteries. iv) Four RPs provide for a degree of redundancy that allows for easy automatic detection of erroneous distance measurements through a computed parameter.

Section II is devoted to the description of the operating principle and on the architecture of the positioning system, with focus on the specific advantages of the design choices. Section III presents

the system realization while in Section IV the experimental results are shown and discussed. The last section draws the conclusions of this work.

II. System Operating Principle and Architecture

In this Section, the positioning system operating principle and architecture are described.

A - Trilateration

The proposed system measures the distances from suitable RPs to a multiplicity of mobile units (MUs) and calculates the position by the intersection of spheres having radius equal to the distances between MUs and RPs. The intersection of four spheres in 3D space, with the constraint that their centers must be non-coplanar, identifies the position of a point in space in a unique manner (see Fig. 1). The position $X_j = (x_j, y_j, z_j)$ of the j^{th} MU can be estimated, in absence of bias or random errors, as solution of the following spheres' intersection:

$$\begin{cases} l_{1j}^2 = \left(x_j - x_{RP1}\right)^2 + \left(y_j - y_{RP1}\right)^2 + \left(z_j - z_{RP1}\right)^2 \\ l_{2j}^2 = \left(x_j - x_{RP2}\right)^2 + \left(y_j - y_{RP2}\right)^2 + \left(z_j - z_{RP2}\right)^2 \\ l_{3j}^2 = \left(x_j - x_{RP3}\right)^2 + \left(y_j - y_{RP3}\right)^2 + \left(z_j - z_{RP3}\right)^2 \\ l_{4j}^2 = \left(x_j - x_{RP4}\right)^2 + \left(y_j - y_{RP4}\right)^2 + \left(z_j - z_{RP4}\right)^2 \end{cases}, \quad (1)$$

where $X_{RPi} = (x_{RPi}, y_{RPi}, z_{RPi})$ is the position of the i^{th} (i = 1, 2,…4) RP and $l_{1j}, l_{2j},\ldots l_{4j}$ the distances between MU and the four RPs.

Some general assumptions allow simplifying the problem. Three RPs identify a plane *P* in space; if it is known a priori that the point to locate belongs to only one of the two half-spaces defined by the plane *P*, therefore such three RPs are sufficient for positioning. This is the practical case of a positioning system in which the RPs' plane lies on the ceiling or on the wall of a room, within which one wants to locate the MU.

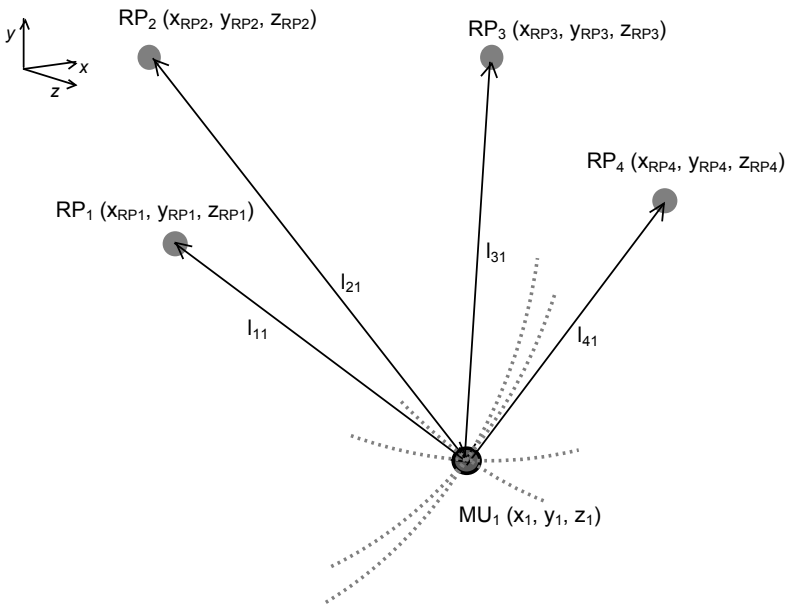

Figure 1. Positioning through four spheres' intersection.

B - Closed form solution of the sphere intersection

Also, if we place four RPs in a coplanar way at the vertices of a rectangle of sides *a* and *b*, so that X_{RP1} = (0, 0, 0), X_{RP2} = (*a*, 0, 0), X_{RP3} = (*a*, *b*, 0) and X_{RP4}= (0, *b*, 0) (see Fig. 2), then we can rewrite (1) as follows:

$$\begin{cases} l_{1j}^2 = x^2 + y^2 + z^2 \\ l_{2j}^2 = \left(x - a\right)^2 + y^2 + z^2 \\ l_{3j}^2 = \left(x - a\right)^2 + \left(y - b\right)^2 + z^2 \\ l_{4j}^2 = x^2 + \left(y - b\right)^2 + z^2. \end{cases} \tag{2}$$

Under the above assumptions, the solution of the system composed of the equations 1, 2 and 4 of the (2) can be written in closed form [21]:

$$\begin{aligned} x_1 &= \frac{l_{1j}^2 - l_{2j}^2 + a^2}{2a} \\ y_1 &= \frac{l_{1j}^2 - l_{4j}^2 + b^2}{2b} \\ z_1 &= \sqrt{\left| l_{1j}^2 - x_1^2 - y_1^2 \right|}. \end{aligned} \tag{3}$$

As a noticeable result, the rectangular arrangement of RPs yields a closed form solution of sphere intersection using only three spheres.

In particular, the four possible closed form solutions of the systems resulting by picking in all combinations three sphere equations at a time from the available four (2) yield four sets of coordinates for the position of the MU:

$$
\begin{aligned}
x_1 &= \frac{l_{1j}^2 - l_{2j}^2 + a^2}{2a} \qquad x_2 = \frac{l_{1j}^2 - l_{2j}^2 - a^2}{2a} + a \\
y_1 &= \frac{l_{1j}^2 - l_{4j}^2 + b^2}{2b} \qquad y_2 = \frac{l_{2j}^2 - l_{3j}^2 + b^2}{2b} \\
z_1 &= \sqrt{\left| l_{1j}^2 - x_1^2 - y_1^2 \right|}, \; z_2 = \sqrt{\left| l_{2j}^2 - \left(x_2 - a\right)^2 - y_2^2 \right|}, \qquad (4) \\
x_3 &= \frac{l_{4j}^2 - l_{3j}^2 - a^2}{2a} + a \qquad x_4 = \frac{l_{4j}^2 - l_{3j}^2 + a^2}{2a} \\
y_3 &= \frac{l_{2j}^2 - l_{3j}^2 - b^2}{2b} + b \qquad y_4 = \frac{l_{1j}^2 - l_{4j}^2 - b^2}{2b} + b \\
z_3 &= \sqrt{\left| l_{3j}^2 - \left(x_3 - a\right)^2 - \left(y_3 - b\right)^2 \right|}, \; z_4 = \sqrt{\left| l_{4j}^2 - x_4^2 - \left(y_4 - b\right)^2 \right|}.
\end{aligned}
$$

It should be noted that each set of three equations (4) has two possible solutions for z_h (h = 1, 2,…4), where a single solution is obtained by limiting the positioning to the half-space in front of the reference set corresponding to $z_h > 0$. The existence of a closed form solution due to the particular arrangement of the RPs at the vertexes of a rectangle considerably reduces the computational load required for the calculation of the position and even makes it possible to calculate the position on board of small battery-powered MUs. In general, a number of RP larger than three yields a resolving system that can be linearized, and then solved with a matrix closed form instead that heavy iterative methods [13], but in such case the RPs can not be coplanar. The non-coplanarity sets strict limits on the integrability of such structures in ceilings or walls.

C – RPs' arrangement advantages

The four solutions are numerically identical only if the distance measurements are not affected by error. In any case, in practice, each distance measurement is unavoidably affected by the quantization error of the distance measurement and by other errors. Moreover, since the distance error is propagated through the formulas (3) on positioning with a magnitude that depends on the relative position of the MU in space with respect to the RPs (see below Section IV.B), it is evident that the four solutions will differ by a certain extent. However, they are expected to be very close to each other, and if not, it can be assumed that at least one measurement error occurred.

The use of four RPs, in place of the three just sufficient for positioning through (3), shows multiple advantages. First, the existence of a fourth RP adds a certain degree of redundancy to the system, which makes it possible to recognize situations in which there is at least one error in the four distance measures, for example caused by the presence of an obstacle blocking the line of sight between MU and one of the RPs. On the contrary, it should be noted that each of the four equation sets (4) still outputs a set of coordinates for the MU even when one or more distance measures are incorrect, so providing a fake position. The developed algorithm incorporates a technique for identifying and discarding any erroneous distance estimate that would result in the miscalculation of the MU position. To this purpose, the Euclidean distance D between the four computed MU positions using (4) is calculated as the square root of the sum of squared differences between every pair of coordinates out of the four computed sets of coordinates of the MU:

$$D = \sqrt{\sum_{\substack{h,k=1 \\ k>h}}^{4} \left(x_h - x_k\right)^2 + \sum_{\substack{h,k=1 \\ k>h}}^{4} \left(y_h - y_k\right)^2 + \sum_{\substack{h,k=1 \\ k>h}}^{4} \left(z_h - z_k\right)^2} . \tag{5}$$

In summary, D represents the summation of the distances between the six combinations of two out of the four points generated by the equations (4). If one or more distance measurements are incorrect, D is greater than a given threshold value. In this case, the calculated current position of the MU is incorrect and therefore discarded. It should be noted that this mechanism does not overcome the necessity to have always a line of sight between the MU and all the four beacons, but

it is capable to signal to the system the presence of an error. A suitable value of D can be found through a try-and-error procedure.

Second, the position of the j^{th} MU can be calculated as an average of the four positions computed by (4), making it more robust against small and unbiased errors on the estimates of the four distances:

$$\begin{cases} x_j = \frac{1}{4}\sum_{h=1}^{4} x_h \\ y_j = \frac{1}{4}\sum_{h=1}^{4} y_h \\ z_j = \frac{1}{4}\sum_{h=1}^{4} z_h. \end{cases} \quad (6)$$

Thirdly, the coplanar arrangement of the four RPs makes it easy to place them within the normal architectural elements of a room, for example to replace a normal square panel of a false ceiling.

D - Time of Flight and distance estimation

Each distance measurement is performed by measuring the *ToF* of an ultrasonic linear chirp traveling from an emitter, or beacon, located in one of the RFs, to the MU. The signal received by the MU is time sampled and cross-correlated with a reference signal stored in the memory of a processor on-board the MU itself, and the *ToF* is finally detected, which is proportional to the position of the cross-correlation peak. When the *ToF* is estimated through the cross-correlation peak, the beacon-MU distance is computed taking into account the sound speed in air. The distance measurement accuracy of the order of the current space sampling (i.e. the distance covered by the ultrasound during the time sampling interval) can be achieved, since the space sampling can be made much smaller than the ultrasound wavelength. Chirp signal shows a very sharp auto-correlation peak, and the wider the chirp bandwidth the narrower the peak. The temporal resolution is inversely proportional to the bandwidth and duration of the chirp. Additionally, the cross-correlation greatly increases the Signal-to-Noise Ratio (SNR), provided signal and noise are uncorrelated. As possible drawback, the cross-correlation peak of the line-of-sight travelling chirp

is not always the highest peak. Sometimes, in fact, a number of signals coming from indirect paths, or echoes, combine each other to form a received signal having late cross-correlation peaks, nevertheless higher in amplitude in respect to that associated with the direct path signal. Only the direct path related cross-correlation peak gives the correct *ToF*. The earliest and true cross-correlation peak can be found by using some search mechanism [17], [22].

To carry out the four required measurements, the same signal is emitted in turn by the four beacons. In open space, we can assume that the *ToF* t_{ij} is proportional to the distance l_{ij} between the RP i^{th} (i = 1, 2,…4) and the MU j^{th} (j = 1, 2,…M), and inversely proportional to the current average speed of the sound c_{air} along that path, according to:

$$l_{ij} = c_{air} t_{ij} + l_{so}, \tag{7}$$

where

$$c_{air} = 331.5\sqrt{1 + \frac{T}{273.15}} \tag{8}$$

is the speed of sound (m/s) in air at the ambient temperature T (°C) and l_{so} is the offset introduced by the system delays, including beacon-MU synchronization jitter.

This work aims to present a 3D positioning with a few centimeters accuracy within a 4×4×3 m^3 volume, e.g. a standard room.

Considering the propagation of the measurement error through the positioning calculations, to obtain an accuracy of positioning of the order of centimeters, measurement accuracy of the order of millimeters is required, as discussed in Section IV.B.

The distance between the RF and the MU is estimated by measuring the *ToF* of an ultrasonic linear chirp traveling from a beacon placed in a RP to a receiver onboard the MU. The *ToF* of a signal traveling between an emitter and a receiver is calculated by subtracting the emission time from the arrival time. A ranging accuracy of few millimeters requires the emitter and receiver timers synchronized with a worst-case few microseconds jitter.

A ranging system synchronized through the well-developed communication standard ANT has been

already proposed by the authors [22]. In summary, synchronization through a direct message between a transmitter and a receiver is not possible using existing and well-developed RF communication standards such as Bluetooth, ANT or WiFi. In fact, ANT and other similar standards do not allow knowing a priori the exact delay between the transmission time of a specific message and the reception time of that message by the listener. Moreover, the experimental time delay shows uncertainty of the order of hundreds of microseconds [23].

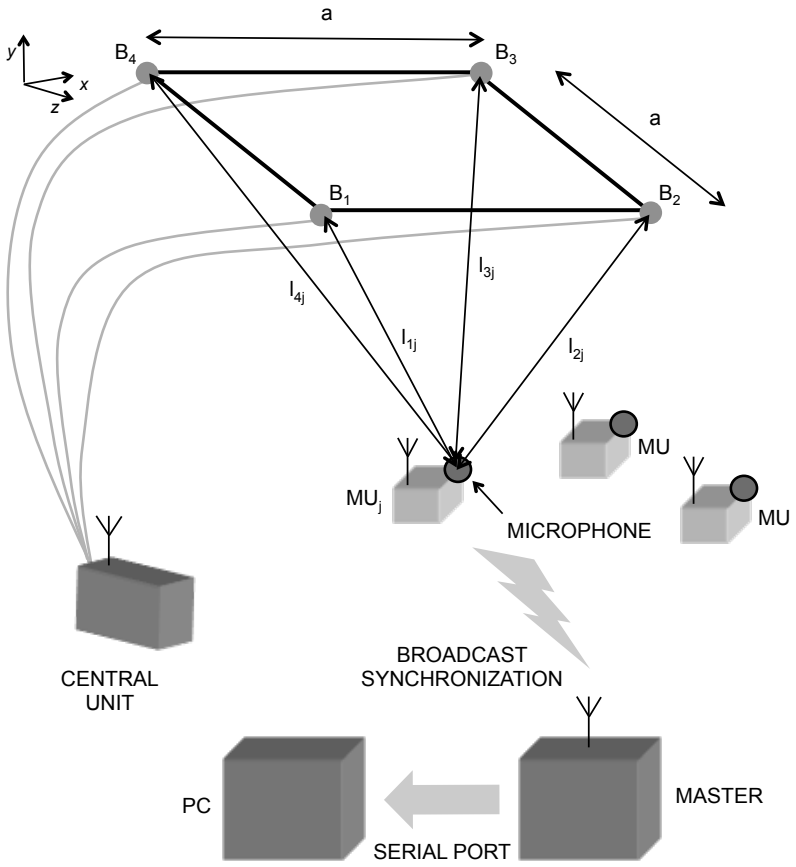

Figure 2. System Architecture. The Master Unit synchronizes Central Unit and multiple MUs with an RF broadcast message; the Central Unit emits the ultrasonic chirp signals through the four beacons B_1, B_2,...B_4; each MU receives the four ultrasonic signals and calculates its own position. If required, the Master Unit downloads the MUs' positions and communicates them to a PC via serial port.

The Broadcast-Reference Synchronization technique [24] overcomes this obstacle by involving a sender that sends a broadcast message to a multiplicity of receivers that noticeably receive the message at the same time. In this way, the synchronization is done among the receivers each other, which share the receiving time instant, but not between sender and receivers. Experimental tests

showed that using this technique, a time difference or jitter limited to 3 μs between the timers of multiple receivers is achieved. Assuming a sound speed of 343 m/s, 3 μs corresponds to a ranging uncertainty of 1.03 mm, which is acceptable for the applications foreseen.

Following the previous considerations, the synchronization mechanism described in [22] for a ranging system is exploited in the proposed positioning system, as explained hereafter.

E - System Architecture

In Figure 2 it is shown a schematic of the system. Four co-planar beacons B_1, B_2…B_4 are placed at the vertexes of a square of side *a*, having coordinates X_{RP1} = (0, 0, 0), X_{RP2} = (*a*, 0, 0), X_{RP3} = (*a*, *a*, 0) and X_{RP4}= (0, *a*, 0), respectively. A Master Unit, featuring ANT, acts as message sender while a Central Unit and multiple MUs act as message receivers (see Fig. 2), all including an ANT module, which therefore are synchronized. The Central Unit emits the ultrasonic chirp signals through the four beacons B_1, B_2,…B_4 in sequence toward a multiplicity of MUs within a given 3D space region. Each MU, upon the Master's RF synchronization signal, starts the acquisition of the whole sequence of the four ultrasonic signals along a suitable listening window sampling and digitizing the incoming signals. The signal acquisition is followed by the cross-correlation with the stored chirp, the detection of the four peaks, the computations of the four *ToF*s and related ranges, and finally by the calculation of the coordinates using (4). Fig. 3 shows a high-level flow-chart of the internal MU operation sequence.

It is worth noting that the proposed system architecture allows an unlimited number of autonomous MUs.

The Master Unit, if required, can download via ANT protocol the position coordinates from the MUs and communicate them to a PC using a suitable serial connection, e.g. for position display or tracking purpose. In such case, a specific protocol is in charge of handling data download of a limited number of MUs (see [22] for details).

III. System Realization

The system is designed to cover an average house or office room of 4×4×3 m^3, where the beacons' square set is placed nearby the ceiling center.

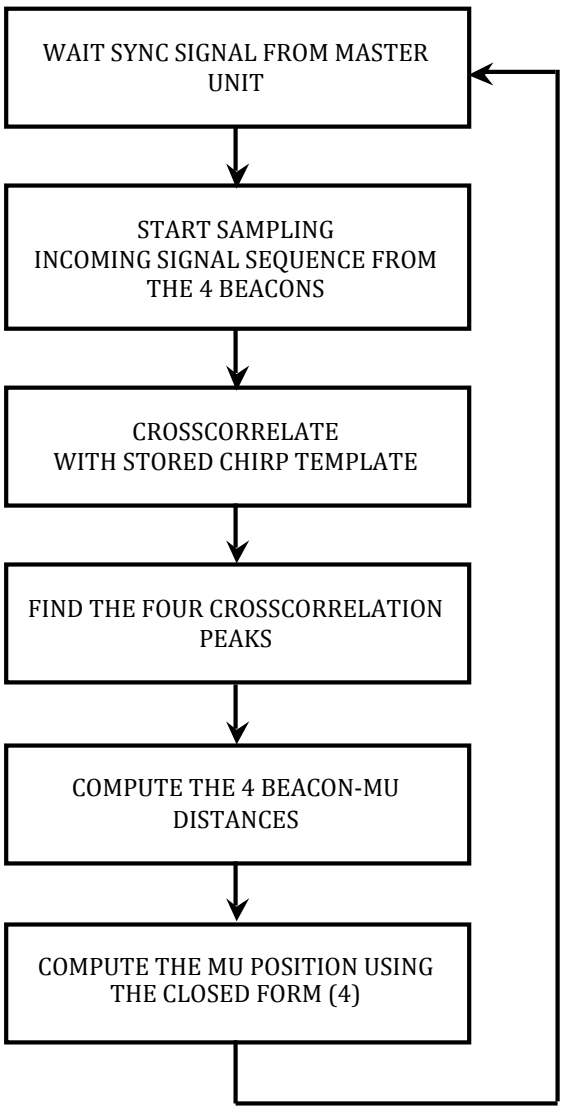

Figure 3. Operation flow-chart of a Mobile Unit. Upon the synchronization signal from the Master Unit, the MU starts the acquisition of a signal with duration equal to the time required by the sequence of four beacon emissions and related listening windows. The signal acquisition is followed by the cross-correlation with the stored chirp, the detection of the four peaks, the computations of the four *ToF*s and related ranges, and finally by the calculation of the coordinates using (4).

A - Master Unit

The Master Unit consists of a N5 module (Dynastream Innovations, Cochrane, Alberta, Canada) connected to a PC via UART/USB interface. The N5 includes a chip nRF51422 (Nordic Semiconductor ASA, Oslo, Norway), equipped with a 16 MHz ARM Cortex M0 processor, and a radio supporting 2.4 GHz communication protocols ANT [23] or Bluetooth Smart (see Figure 4). It is important to notice that the communication from the MUs to the Master Unit and the PC connection are used only in order to read and display the positioning data, otherwise the MUs operate autonomously and privately, e.g. like GPS mobile units.

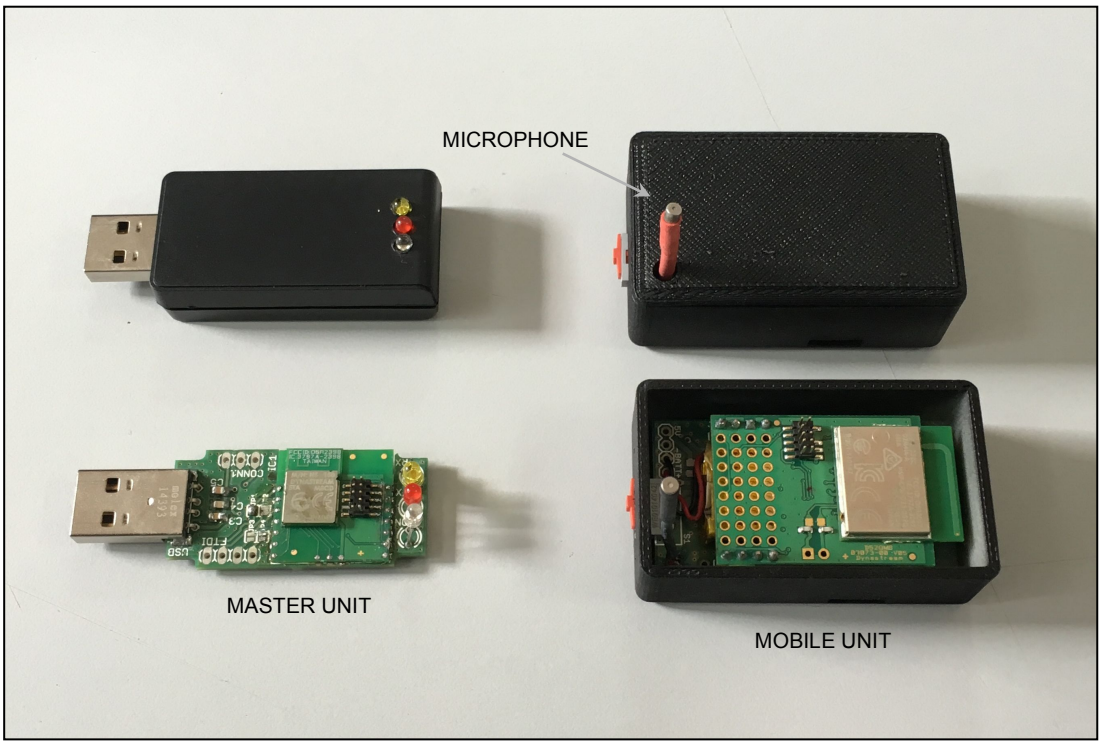

Figure 4. Realized Master Unit and Mobile Unit: Master Unit includes N5 module and UART/USB interface with and w/o plastic shell (left); Mobile Unit includes microphone, signal conditioning, D52 module and lithium-ion battery, with and w/o plastic shell (right).

B - Mobile Unit

The Mobile Unit is equipped with a D52 module (Dynastream Innovations, Cochrane, Alberta, Canada) built around the nRF52832 chip (Nordic Semiconductor ASA, Oslo, Norway), which

includes a 12-bit ADC set at 200 kSamples/s and features a 64 MHz ARM Cortex M4, all powered by a 3.7 V 30×17×5 mm^3 rechargeable lithium-ion battery with capacity 250 mAh.

The MU includes a miniature microphone FG-6163 (Knowles Acoustics, Itasca, Illinois, USA) with length and diameter 2.6 mm, acoustical receiving window diameter 0.79 mm, which is amplified and filtered by a linear circuitry, with no AGC [25], based on OPA2835 (Texas Instruments Inc., Dallas, Texas, USA) (see Figure 4).

C - Central Unit and Beacons' Set

The Central Unit is composed of a N5 module and of a microcontroller PIC16F1704 (Microchip Technology Inc., Chandler, AZ, USA), for the ultrasonic chirp storage and output through the built-in 8-bit DAC. A linear up-chirp in the bandwidth 30-50 kHz is employed. The chirp signal is composed of 612 samples at 239 kSamples/s Hanning windowed to avoid audible "clicking", with a total duration of 2.56 ms. The chirp is amplified and fed to a Class AB MOSFET power amplifier. The chirp is then fed in sequence to the four beacons through the switch bank composed of two 2-channel MAX4690 (Maxim Integrated, San Jose, CA, USA). In each of the four output channels, the chirp signal level is further raised to 300 Vp-p with a signal voltage elevator realized using the miniaturized 1:100 coil transformer LPR6235-752S (Coilcraft, Glasgow, UK). The ultrasonic transducers are Series 7000 Electrostatic Transducer (SensComp Inc., Livonia, MI, USA) [26]. The capacitive transducers are DC-biased by 200V supplied by the ultra-miniature DC to HV DC Converter Q02-5-R (EMCO High Voltage Corp., Sutter Creek, CA, USA).

Series 7000 transducers have not been designed for this application and need adaptation. In fact, their emission cone (far field) is rather narrow. The emission cone semi-angle ϑ is approximately described in far field by the well-known relationship [27]:

$$\sin\vartheta = 1.22\frac{\lambda}{D}, \tag{9}$$

where λ is the emitted wavelength and D the diameter of the circular transducer. Since the emitted signal is a chirp, the narrowest emission cone occurs at the highest frequency of the chirp signal, i.e. 50 kHz. At that frequency and with the Series 7000 aperture D = 20 mm, according to (9) ϑ is 24.7°. However, this result can be slightly different from the datasheet emission diagram, which is carried out not in full far field conditions [26].

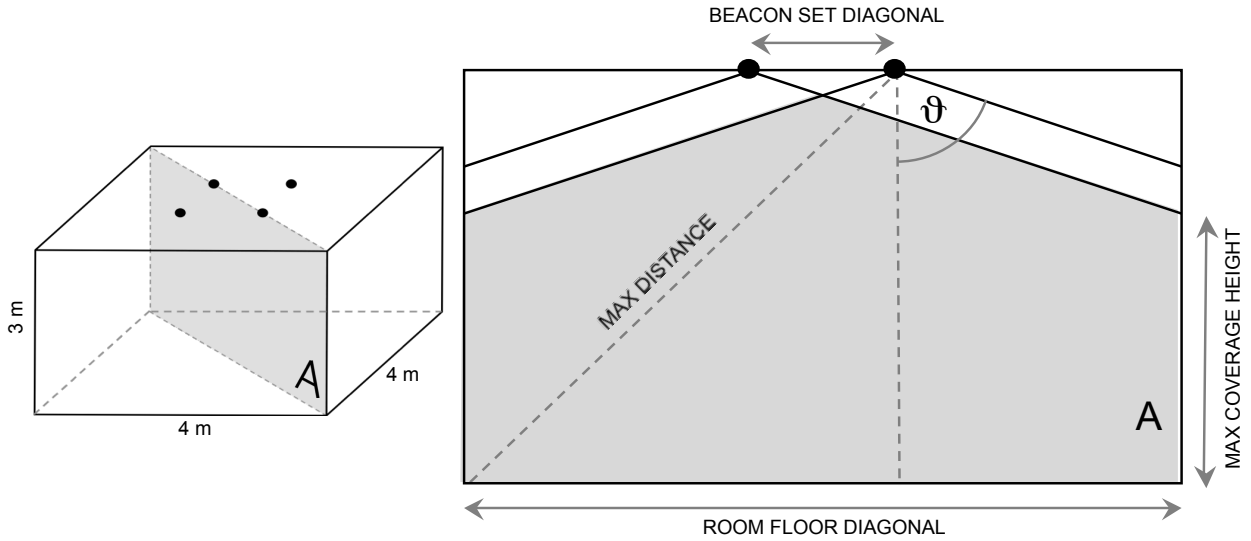

Figure 5. Beacon set placement and covered room volume (grey region) with room size 4×4×3 m^3, beacon square frame side 0.5 m and transducers' semi-cone aperture ϑ = 80.95°. Axonometric view (right, not in scale) and diagonal section A (left, not in scale).

The system has been designed to cover the volume of the room from the floor up to 2.5 meters in height. Figure 5 (not in scale) shows the floor-ceiling section along the diagonal of the 4×4×3 m^3 room considered in the system dimensioning. The system operating volume is that covered by all the four beacons at the same time. With the measures considered, the desired volume coverage occurs with $\vartheta \geq 80.95°$.

To obtain such wide angle, according to (9), the aperture diameter has been reduced to 8.5 mm. This was accomplished by placing in front of the transducer an acoustical mask with a circular hole with diameter 8.5 mm. This arrangement shows some side effects that reduce the transducer performance: the presence of the mask reduces the emitted acoustic power and, depending on the shape and size of the cavity formed by the transducer/mask assembly, some resonance frequencies

may appear within the transducer used band. However, an extensive study of the acoustical effects of the aperture modification is beyond the scope of this work. Our experiments show that these side effects do not prevent the proper operation of the system.

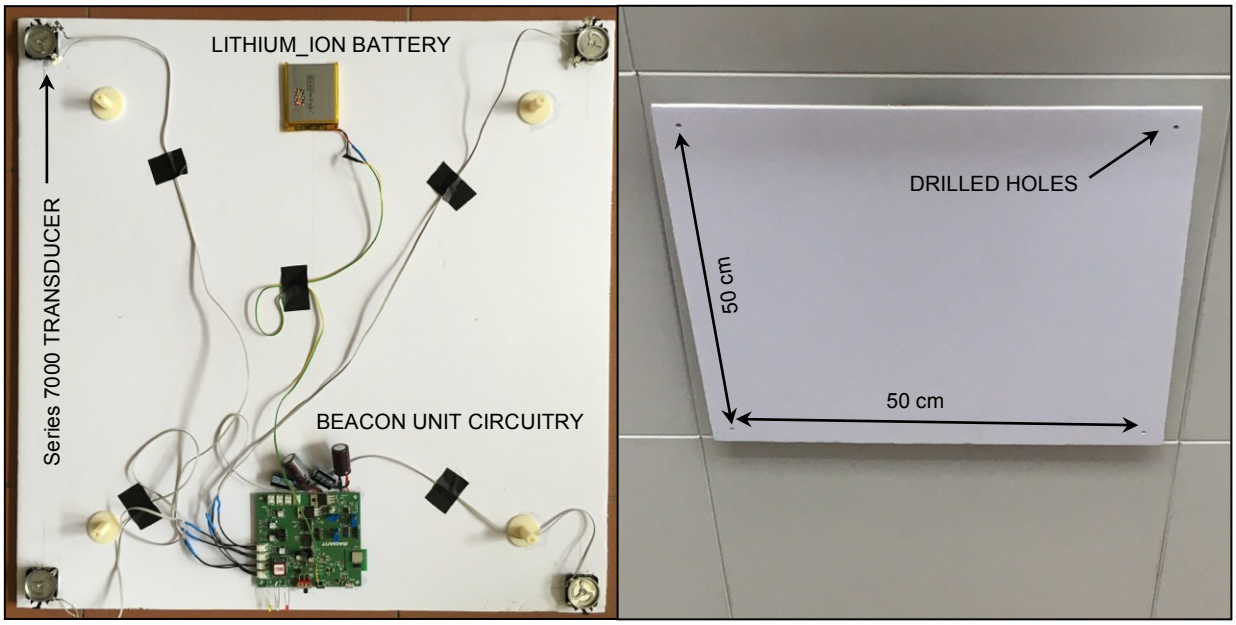

Figure 6. Beacon Unit: a) backside view of the false ceiling panel hosting four capacitive SensComp Series 7000 transducers, N5, PIC16F1704, preamplifier, power amplifier, voltage elevator, and polarization circuitry The Unit is power supplied by a lithium-ion battery. b) Front side view of the false ceiling panel with the four drilled holes with diameter 8.5 mm for airborne chirp emissions. The Unit is placed just below the room false ceiling using double-sided adhesive tape.

The Beacon Unit components are mounted on the backside of a square 52×52 cm^2 panel. The four transducers are placed at the vertex of a 50×50 cm^2 square, face down toward the room volume (see Fig. 6).

Ultrasonic signals are emitted through four 8.5 mm diameter holes. The panel backside hosts all the circuitry plus a 3.7 V 50×60×5 mm^3 rechargeable lithium-ion battery with capacity 2000 mAh. Furthermore, three LEDs display the on/off state, the wireless connection to the Master Unit, and, by flashing, the cyclic emission of the chirp signals.

IV. Experimental Results and Discussion

A - Ranging summary

Positioning is computed from four distance measurements between four beacons at RPs and a multiplicity of MUs. Each distance measurement is carried out by measuring the time of flight of an ultrasonic chirp traveling from one at a time emitting beacon to receiving MUs. It requires a tight synchronization between the beacon emission and the MUs, which in this work is carried out by using the Broadcast-Reference Synchronization technique [24] and miniature commercial modules featuring ANT WPAN communication plus an onboard microprocessor [23]. The time jitter achieved is less than 3 μs, which translates in a maximum distance uncertainty of 1.03 mm assuming sound speed 343 m/s [22].

Positioning requires four distance measurements in sequence between the four beacons and the MU. In order to reach the furthest points within the given room volume, which actually are the 4.37 m distant bottom corners of the room from at least one beacon, each measurement duration is set 15.3 ms, a value obtained by adding to the longest expected *ToF* the chirp duration (here 2.56 ms), assuming a speed of sound in air of 343 m/s.

However, the sensor must sample the signal for an overall listening window four times longer (61.2 ms), so as to store the incoming chirp complete sequence.

In the experiments that will follow SNR = P_{signal}/P_{noise}, where P_{signal} and P_{noise} are the powers of signal and noise, respectively, decreases from approximately 23 dB at a range of 1 meter to 0 dB at a range of 4.37 meters. It is due to spherical spreading and air attenuation according to [28], where an extensive power budget analysis for ultrasound localization systems is carried out. Even with such low SNR, reliable peak detection is still possible thanks to the cross-correlation gain.

B - Accuracy bound and reliability remarks

The mean squared error lower bound ε_{MSE} for the time accuracy detection of the time delay is given by the Cramér-Rao formulation [29]:

$$\varepsilon_{MSE} \geq \frac{\pi}{WT\omega_0^2 SNR}, \tag{10}$$

where WT is time-bandwidth product, ω_0 is the center pulsation (rad/s) and SNR is the signal-to-noise ratio. According to [29], equation (10) holds for SNR > SNR3, i.e. when SNR is high enough to have no ambiguity in the peak detection. SNR3 is defined by:

$$SNR3 = \frac{6}{\pi^2 \frac{WT}{2\pi}} \left(\frac{\omega_0}{W}\right)^2 \left[\varphi^{-1}\left(\frac{\omega_0^2}{24W^2}\right)\right]^2. \tag{11}$$

In the present case, considering the following reasonable values $B = 20$ kHz, $T = 2.6$ ms, $f_0 = 40$ kHz, $SNR = 1$ (worst case 0 dB @ 4.37 m), and therefore $W = 125.66 \cdot 10^3$ rad/s and $\omega_0 = 251.33 \cdot 10^3$ rad/s, then SNR3 is ≈ -6dB, which is a value smaller than our worst 0 dB @ 4.37 m. Therefore, in the present case it is justified to use (10), from which it turns out that $\varepsilon_{MSE} \geq 1.52 \cdot 10^{-13}$ s. Assuming the sound velocity 343 m/s at 20 °C, the distance error lower bound results 133 μm.

It is interesting to notice that SNR3 is inversely proportional to WT, thus taking into account the processing gain from the observation window of duration T, in our case due to the cross-correlation processing.

However, we previously mentioned that the ultrasound signal is sampled on-board the MU with 5 μs time resolution. The time accuracy of our prototypal system is limited by its sampling rate and, without subsample interpolation [30], it cannot be shorter than the duration of one clock period. The highest available range accuracy of the presented system is therefore given by $p = vT_S$, where p is the accuracy margin in meters, v the sound speed and T_S the time between two successive samples. At 20 °C, this margin is equivalent to 1.7 mm, which is much greater than the Cramér-Rao bound above found.

The measurements ideally should be done simultaneously, especially if the MU is moving. Otherwise, the four distance measurements will be carried out for different MU positions, producing a position error that increases with the velocity of the MU.

Strong temporary acoustic disturbances (such as objects falling on the floor, slamming doors, etc.) and variations in the speed of sound due to changes in humidity, thermal drift and air mass flow, are among other potential causes of inaccurate distance estimation (and position estimation through (4)).

Although the causes of error are several, here for simplicity only the effect of quantization error is presented. The quantization error has a uniform distribution and, from an engineering point of view, it is useful to know the worst-case error, which is the maximum error that can be made on each coordinate.

Briefly, considering the functional relationship $y = f(x_1, x_2,\ldots x_k)$, small changes Δx_1 in x_1, Δx_2 in $x_2,\ldots$, Δx_k in x_k, all propagate to produce a worst-case small change Δy in y in the following manner:

$$\Delta f \cong \sum_{j=1}^{k} \left| \frac{\partial f}{\partial x_j} \right|_{x_j = x_{j0}} \Delta x_j. \tag{12}$$

The use of the partial derivative module takes into account the fact that in the worst case the contributions relating to each of the independent variables are added together.

Equation (1) is used when it is not given to repeat a sufficiently high number of measures (> 10) to estimate the average quadratic error. We are considering a MU that does not stay fixed in space, so that generally the measurement at a given spatial point is single. Equation (1) is actually an approximation, since any higher order terms such as $(\Delta x_1)^2$ have been set to zero. However, this approximate form is sufficiently accurate for most purposes. The derivatives $\partial f/\partial x_1$, $\partial f/\partial x_2$, etc., are given numerical values when evaluated at the actual experimental values of $x_1 = x_{10}$, $x_2 = x_{20}$, etc., and so these derivatives are effectively constants.

For this analysis, we can limit ourselves to considering the localization with three emitters. The fourth serves to determine the validity of the measure and to decrease the location error through

averaging. According with (3), the functions to be considered are three, one for each spatial coordinate (x, y, z), depending on the emitter-sensor distance measurements l_1, l_2, l_3. By applying (12) to (3), it is therefore obtained:

$$\begin{aligned}
\Delta x &\cong \left|\frac{\partial x}{\partial l_1}\right|\Delta l_1 + \left|\frac{\partial x}{\partial l_2}\right|\Delta l_2 = \left|\frac{l_1}{a}\right|\Delta l_1 + \left|\frac{l_2}{a}\right|\Delta l_2 \\
\Delta y &\cong \left|\frac{\partial y}{\partial l_1}\right|\Delta l_1 + \left|\frac{\partial y}{\partial l_2}\right|\Delta l_2 = \left|\frac{l_2}{b}\right|\Delta l_2 + \left|-\frac{l_3}{b}\right|\Delta l_3 \\
\Delta z &\cong \left|\frac{\partial z}{\partial l_1}\right|\Delta l_1 + \left|\frac{\partial z}{\partial l_2}\right|\Delta l_2 + \left|\frac{\partial z}{\partial l_3}\right|\Delta l_3 = \left|\frac{-l_1 x}{az}\right|\Delta l_1 + \left|\frac{l_2}{z}\left(\frac{x}{a} - \frac{y}{b} + 2\right)\right|\Delta l_2 + \left|\frac{l_3 y}{bz}\right|\Delta l_3,
\end{aligned} \tag{13}$$

where Δl_j is the quantization error of the measurement of the sensor emitter distance. In the worst case, Δl_j is equal to the whole quantization interval, i.e. $\Delta l_j = vT_s$, where v is the speed of the sound in air and T_s the sampling period. In (13), the resulting values must be considered values that cannot under any circumstances be exceeded, and not as standard deviations. On the other hand, the typical practical value may be smaller but reasonably of the same order of magnitude.

Δx and Δy are proportional to the distance beacon-MU, while Δz explicitly depends on the MU x and y coordinates. In our experimental setup, l_i (i = 1, 2, 3) is limited to 4.37 m, and $a = b$ = 0.5 m, and $\Delta l_i \leq 1.7$ mm. At the furthest point P3 = (2.5, 2.5, 1) (see Fig. 8), where $l_1 = 4.04$ m, $l_2 = 3.76$ m, $l_3 = 3.45$ m, (13) yields $\Delta z = 3.52$ cm, $\Delta x = 2.68$ cm and $\Delta y = 2.47$ cm, respectively. Δx, Δy and Δz must be regarded as upper bound of the real error, which occurs only in the worst case when all the Δl_is assume their maximum value, equal to 1.7 mm, at the same time. Equation (13) shows that to obtain a positioning accuracy of the order of centimeters, measurement accuracy of the order of millimeters is required.

C - Experimental results

Two squared grids of 3×3 test points at steps of 1 m along the x and y axes with horizontal step 1 m, at z = 1 and z = 2.5, respectively, were measured. The MU was placed on a tripod and manually

positioned using a tape meter (see Fig. 7). The grids are shown in Figure 8. During the experiments, the sound velocity was assumed to be constant at 344.6 m/s (T = 22.0 °C).

In order to discover faulty measurements in the positioning test and to evaluate the reliability of the proposed system, each measurement was repeated 100 times. As a result, no abnormalities were measured and no outliers were eliminated. The MU coordinates measured by the system are in good agreement with the ones measured using the manual tape meter (see black circles in Fig. 8).

Figure 7. The MU used for the point grid measurement with its stand at z = 1.

Uncertainty is mainly due to synchronization jitter, which is range independent, to distance measurement errors propagated through (4), and secondarily to system time sampling and manual measurement limitations.

In Figure 9, the experimental results of a single positioning operation for all the points on the grid are plotted. In particular, the positioning error is computed as the Euclidian distance from the true point and the measured one.

Figure 10 shows the mean subtracted values of the experimental results of 100 repetitions of the positioning of a single test point on the grid.

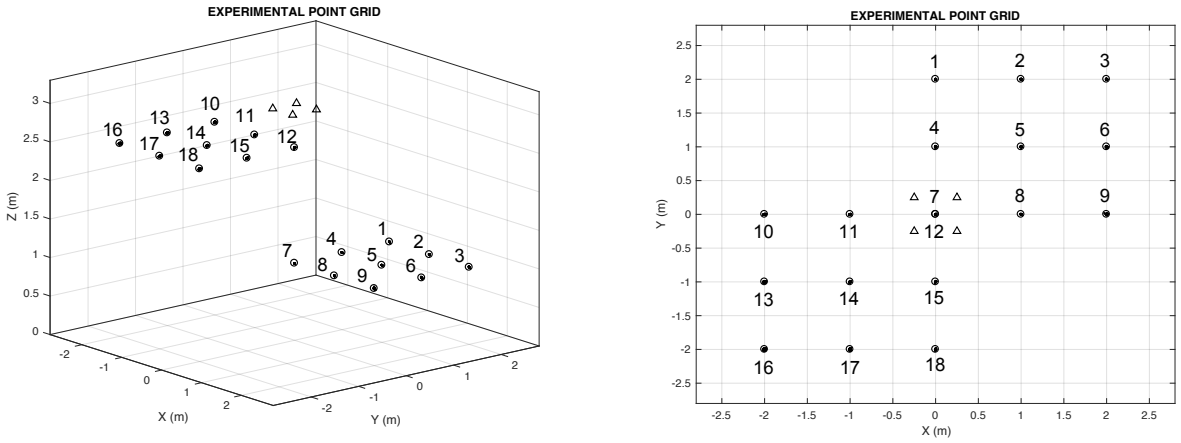

Figure 8. Two views of the experimental positioning: beacons (triangles), point grid of true points (circle) and measured positions (dots). Due to the four beacons placement symmetry, it is sufficient to measure only a quarter of the covered region. In particular, two quarters were measured, at z = 1 m and at z = 2.5 m, respectively. Near each point is shown its consecutive number.

As highlighted in the introduction, the positioning system is designed for a real-time use, so in practice there is no time to average multiple measurements.

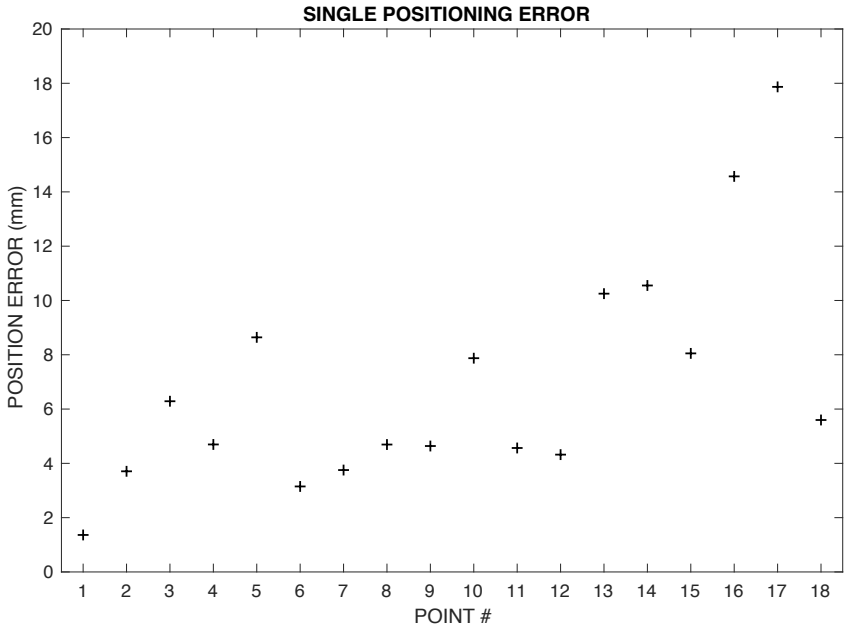

Figure 9. Single positioning operation error at the 18 points of the grid (z = 1 m and z = 2.5 m) shown in Fig. 8.

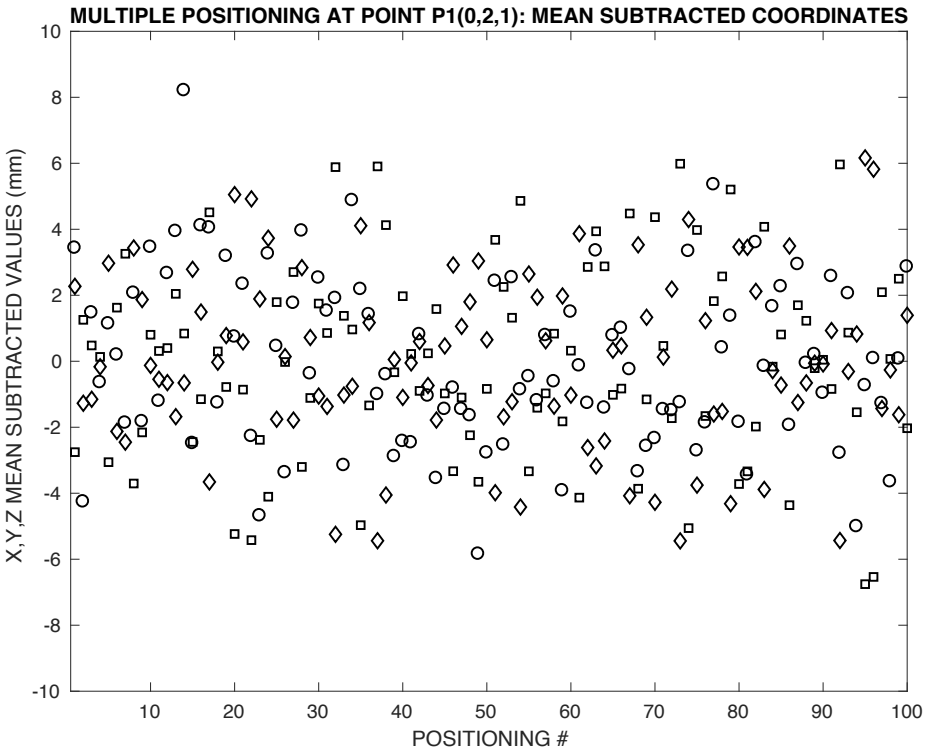

Figure 10. Experimental results of 100 repetitions of the positioning at the point P1 at coordinates (0, 2, 1): mean subtracted values of X (circles), Y (squares) and Z (diamonds).

The plots of the mean subtracted values of the *x*, *y*, and *z* coordinates at point P1 show a good stability of the overall positioning process along time.

Using the complete measurement data set (100 measurements per each position), the standard deviation of the Euclidean positioning error was computed, which for all of the 18 measured points was below 6 mm (see Figure 11), where the positioning error is assumed as the Euclidean distance between the ground truth position and the related system measurement.

In Figure 12 is shown the cumulative error distribution (CDF) of the positioning data of the point (0, 0, 1) (most favorable case), together with the cumulative error distribution of the positioning data of the point (2, 2, 1) (furthest point worst case) over the 100 positioning measurements. Figure 12 shows that the positioning errors for all the measurements are lower than 1.4 cm.

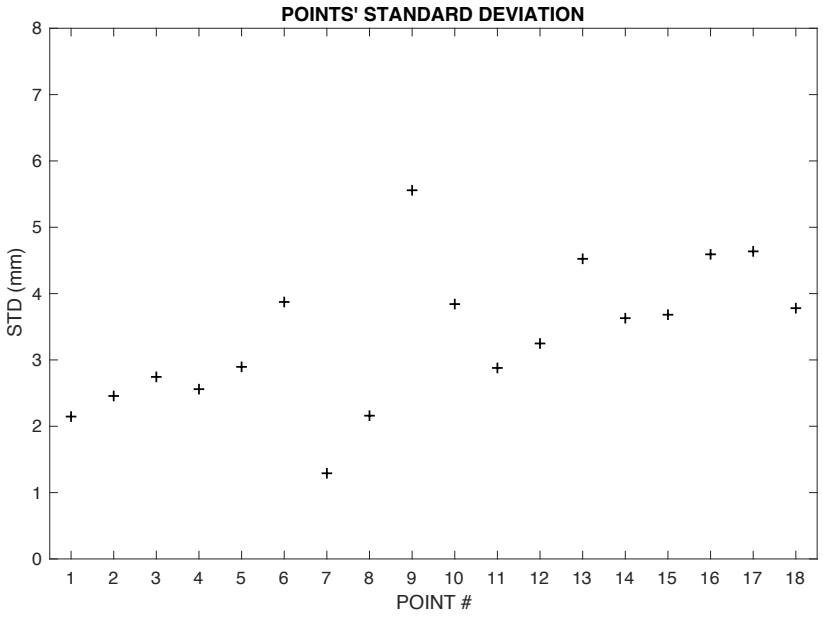

Figure 11. Standard deviation of the 100 range measurements for each of the 18 positions at z = 1 and z = 2.5 on the 4×4 m^2 grid of Fig. 8. Point #7 is the point below the beacons' square center, namely the most favorable position.

A positioning rate of 2 Hz has been achieved, actually limited by the computational power of the D52 processor. The measured average MU power consumption was 21.7 mW.

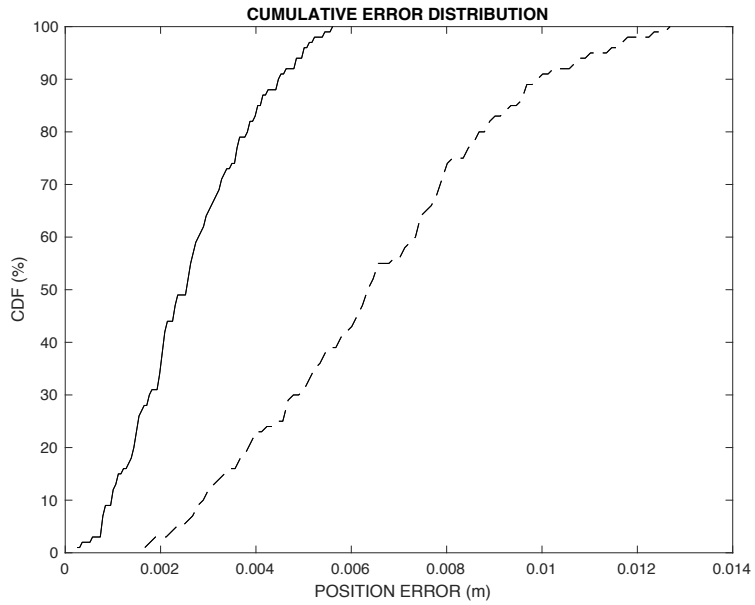

Figure 12. Cumulative error distributions (percent of readings with error less than the value of a given abscissa) of the positioning of the central point (nearest point) (solid), and of the corner point (furthest point) (dashed) at z = 1 m.

It is worth noting that all the MU circuitry, such as ultrasound microphone, analog conditioning, RF module and microcontroller, could be easily realized using an ultra low power technology and designed as a single system-on-chip (SoC).

V. Conclusions

An indoor ultrasonic system for autonomous MU 3D positioning with new relevant features has been proposed and demonstrated. Four beacons are arranged as the vertex of a square. Such flat arrangement allows a closed form solution of the sphere intersection required in the position computation, as well as an easy integration in room false ceiling. Moreover, the flat four-beacon arrangement provides redundancy for detection of positioning errors. Thanks to the closed form solution, the position is easily computed by a small battery-powered mobile unit autonomously and, if required, in a totally private way. The beacon-sensor synchronization through ANT, the onboard cross-correlation, and the positioning computations are carried out using a small battery. Experimental positioning accuracy is less than 14 mm within an average 4×4×3 m^3 office room. The achieved positioning rate of 2 Hz is limited by the computational power of the specific module used. The system architecture allows an unlimited number of autonomous MUs. Ultrasound frequencies in the range 30-50 kHz, allow commercial and low cost ultrasound components. The MU can be in perspective realized as miniature System on Chip. Possible promising applications include domotics, location-aware IoT smart devices, augmented reality, gaming consoles, gestural interfaces, etc.

Acknowledgments

This work was supported by the Italian MIUR Project PON 03PE_00050_1 DOMUS SICUREZZA.

References

[1] D. Zhang, F. Xia, Z. Yang, and L. Yao, “Localization Technologies for Indoor Human Tracking,” no. 60903153, 2010.

[2] R. J. Przybyla, H. Y. Tang, S. E. Shelton, D. A. Horsley, and B. E. Boser, “3D ultrasonic gesture recognition,” in Digest of Technical Papers - IEEE International Solid-State Circuits Conference, 2014, vol. 57, pp. 210–211.
[3] R. Ionescu, R. Carotenuto, and F. Urbani, “3D Localization and Tracking of Objects Using Miniature Microphones,” Wirel. Sens. Netw., vol. 3, no. 5, pp. 147–157, 2011.
[4] R. Carotenuto and P. Tripodi, “Touchless 3D gestural interface using coded ultrasounds,” IEEE Int. Ultrason. Symp. IUS, pp. 146–149, 2012.
[5] Y. Ebisawa, “A pilot study on ultrasonic sensor-based measurement of head movement,” IEEE Trans. Instrum. Meas., vol. 51, no. 5, pp. 1109–1115, 2002.
[6] H. T. Kasprzak and D. R. Iskander, “Ultrasonic measurement of fine head movements in a standard ophthalmic headrest,” IEEE Trans. Instrum. Meas., vol. 59, no. 1, pp. 164–170, 2010.
[7] J. Torres-solis, T. H. Falk, and T. Chau, “A review of indoor localization technologies : towards navigational assistance for topographical disorientation,” Ambient Intell., pp. 51–84, 2010.
[8] N. B. Priyantha, A. Chakraborty, and H. Balakrishnan, “The Cricket location-support system,” Proc. 6th Annu. Int. Conf. Mob. Comput. Netw. - MobiCom ’00, pp. 32–43, 2000.
[9] A. Marco, R. Casas, J. Falco, H. Gracia, J. I. Artigas, and A. Roy, “Location-based services for elderly and disabled people,” vol. 31, pp. 1055–1066, 2008.
[10] C. Sertatil, M. A. Altinkaya, and K. Raoof, “A novel acoustic indoor localization system employing CDMA,” Digit. Signal Process. A Rev. J., vol. 22, no. 3, pp. 506–517, 2012.
[11] M. Hazas and A. Hopper, “Broadband ultrasonic location systems for improved indoor positioning,” IEEE Trans. Mob. Comput., vol. 5, no. 5, pp. 536–547, 2006.
[12] W. Murphy and W. Hereman, “Determination of a position in three dimensions using trilateration and approximate distances,” Dep. Math. Comput. Sci. Color. Sch. Mines, Golden, Color. MCS-95, vol. 7, p. 19, 1995.
[13] C. L. Lawson and R. J. Hanson, Solving Least Squares Problems. Prentice Hall, 1995.
[14] R. Kaune, “Accuracy studies for TDOA and TOA localization,” 2012 15th Int. Conf. Inf. Fusion, pp. 408–415, 2012.
[15] M. Saad, C. J. Bleakley, T. Ballal, and S. Dobson, “High Accuracy Reference-free Ultrasonic Location Estimation,” IEEE Trans. Instrum. Meas., vol. 61, no. 6, pp. 1561–1570, 2012.
[16] E. Díaz, M. C. Pérez, D. Gualda, J. M. Villadangos, J. Ureña, and J. J. García, “Ultrasonic indoor positioning for smart environments: A mobile application,” Proc. 2017 4th Exp. Int. Conf. Online Exp. exp.at 2017, pp. 280–285, 2017.
[17] A. Ens, L. M. Reindl, J. Bordoy, J. Wendeberg, and C. Schindelhauer, “Unsynchronized ultrasound system for TDOA localization,” IPIN 2014 - 2014 Int. Conf. Indoor Position. Indoor Navig., pp. 601–610, 2014.
[18] R. Queirós, F. Corrêa Alegria, P. Silva Girão, and A. Cruz Serra, “Cross-correlation and sine-fitting techniques for high-resolution ultrasonic ranging,” IEEE Trans. Instrum. Meas., vol. 59, no. 12, pp. 3227–3236, 2010.
[19] H. Piontek, M. Seyffer, and J. Kaiser, “Improving the accuracy of ultrasound-based localisation systems,” Pers. Ubiquitous Comput., vol. 11, no. 6, pp. 439–449, 2007.
[20] J. C. Jackson, R. Summan, G. I. Dobie, S. M. Whiteley, S. G. Pierce, and G. Hayward, “Time-of-flight measurement techniques for airborne ultrasonic ranging,” IEEE Trans. Ultrason. Ferroelectr. Freq. Control, vol. 60, no. 2, pp. 343–355, 2013.
[21] J.M. Martín Abreu, R. Ceres, L. Calderón, M.A. Jiménez, P. González-de-Santos, "Measuring the 3D-position of a walking vehicle using ultrasonic and electromagnetic waves," Sensors and Actuators, vol. 75, pp. 131-138, 1999.
[22] R. Carotenuto, M. Merenda, D. Iero, and F. G. Della Corte, “Using ANT communications for node synchronization and timing in a wireless ultrasonic ranging system,” IEEE Sensors Lett., vol. 1, no. 6, pp. 1–1, 2017.

[23] Dynastream Innovations Inc., “ANT Message Protocol and Usage Rev 5.1.” [Online]. Available: https://www.thisisant.com/resources/ant-message-protocol-and-usage/. [Accessed: 15-Sep-2017].
[24] J. Elson, L. Girod, and D. Estrin, “Fine-Grained Time Synchronization Using Reference Broadcasts,” *Proc. 5th Symp. Oper. Syst. Des. Implement.*, pp. 147–163, 2002.
[25] R. Carotenuto, M. Merenda, D. Iero, and F. G. Della Corte, “Ranging RFID tags with ultrasound,” *IEEE Sens. J.*, pp. 1–1, 2018.
[26] I. SensComp, “SensComp, Inc.” [Online]. Available: http://www.senscomp.com/pdfs/Series-7000-Ultrasonic-Sensor-spec.pdf.
[27] G. S. Kino, *Acoustic Waves: Devices, Imaging, and Analog Signal Processing*, vol. 100. Prentice-Hall, 1987.
[28] S. Holm, “Hybrid ultrasound-RFID indoor positioning: Combining the best of both worlds,” *2009 IEEE Int. Conf. RFID, RFID 2009*, pp. 155–162, 2009.
[29] A. J. Weiss and E. Weinstein, “Fundamental limitations in passive time delay estimation-Part I: Narrow-band systems,” IEEE Trans. Acoust. Speech Signal Process., vol. 31, pp. 472-486, 1983.
[30] L. Svilainis, K. Lukoseviciute, V. Dumbrava, A. Chaziachmetovas, "Subsample interpolation bias error in time of flight estimation by direct correlation in digital domain," Measurement, vol 46, n. 10, pp. 3950-3958, 2013.